Oncothermia Journal 15:77-86 (2015)

Nanoheating without Artificial Nanoparticles Part II. Experimental Support of the Nanoheating Concept of the Modulated Electro-Hyperthermia Method, Using U937 Cell Suspension Model

Gabor Andocs[1], Mati Ur Rehman[1], Qing-Li Zhao[1], Edina Papp[2], Takashi Kondo[1] and Andras Szasz[3]

(1) Department of Radiological Sciences, Graduate School of Medicine and Pharmaceutical Sciences, University of Toyama, Toyama, Japan

(2) Faculty of Information Technology and Bionics, Pazmany P. Catholic University, Budapest, Hungary

(3) Department of Biotechnics, St. Istvan University, Godollo, Hungary

Published: Biology and Medicine 7(4):1000247, 2015 (open access)
http://www.omicsonline.com/open-access/nanoheating-without-artificial-nanoparticles-part-ii-experimental-support-of-the-nanoheating-concept-of-the-modulated-electrohyperthermiamethod-using-u937-cell-suspension-model-0974-8369-1000247.php?aid=60362

Biology and Medicine

Andocs et al., Biol Med (Aligarh) 2015, 7:4
http://dx.doi.org/10.4172/0974-8369.1000247

Research Article Open Access

Nanoheating without Artificial Nanoparticles Part II. Experimental Support of the Nanoheating Concept of the Modulated Electro-Hyperthermia Method, Using U937 Cell Suspension Model

Gabor Andocs[1], Mati Ur Rehman[1], Qing-Li Zhao[1], Edina Papp[2], Takashi Kondo[1] and Andras Szasz[3]*

[1]*Department of Radiological Sciences, Graduate School of Medicine and Pharmaceutical Sciences, University of Toyama, Toyama,Japan*
[2]*Faculty of Information Technology and Bionics, Pazmany P. Catholic University, Budapest, Hungary*
[3]*Department of Biotechnics, St. Istvan University, Godollo, Hungary*

Abstract

There are intensive debates about the effects and mechanisms of radiofrequency (RF) hyperthermia in oncology. We theoretically modelled the mechanism of the nanoheating effect of the RF current at the cellular and subcellular level. Then, we experimentally investigated the mechanism of heating in comparison with selective modulated electro-hyperthermia and water-bath heating conventional hyperthermia (WHT) using the U937 suspension cell line model. The two heating-processes resulted in different distributions of energy-absorption, causing different mechanisms of the thermal processes. Both of the mechanisms are thermal (fit to Arrhenius plot) but the selectively absorbed energy by the plasma membrane rafts and the cell-cell contacts of the cells results in earlier cell-destruction than in case of unselective homogeneous heating. This thermal effect is used for the characterisation of selective heating. The experimental results clearly support the previous theoretical considerations; the cell killing effect can be realised at lower temperature ranges in the case of the modulated electro-hyperthermia (mEHT, trade-name: oncothermia) method than with WHT.

Keywords: U937 cell-line; Modulated electro-hyperthermia; Oncothermia; Nanoheating; Membrane raft; Thermal effect; Selective absorption

Introduction

Living tissue is complexly heterogenic. The processes are mostly chemical reactions, where energy absorption-emission is a central point. The energy liberated by metabolic activity appears in the body-temperature, which is also very heterogenic by its sources, but is averaged by natural heat-conduction and the connected temperature equalisation. Hyperthermia is a thermal process, defined by a temperature-elevation in the target [1]. The mass- or volume-specific energy absorption (defined by the specific absorption rate [SAR]) increases the temperature.

In the definition of hyperthermia, temperature is the obligatory parameter, used for dosing by considering the time for which it was effective [2]. Consequently, the treatment has to be identified by temperature, or at least by the specific energy absorption rate (SAR) in the target. The temperature and the energy-deposition must therefore be controlled.

Electromagnetic energy delivery could be by four not completely independent categories, depending on the coupling of the fields to the object; it could be radiation, inductive, capacitive or galvanic coupling [3,4]. All of the interactions have variability in their absorption processes [5], in addition to the structural variations. Consequently, the SAR has microscopic medley values in the living target.

Temperature is the average energy of the particles involved in the absorption process. This general temperature is composed of the various different microscopic heating areas, which could be equalised by the heat-conduction and convection in their surroundings by various time-characters. The macroscopic temperature is a gross-average of all of the microscopic temperatures and their spread-processes.

There are some very high-temperatures (over the protein denaturation [6] that can be locally concentrated and are relatively short time applications. It is limited to a very small volume by various interstitial methods, including the most popular radiofrequency (RF) ablation techniques. However, most of the hyperthermia practices in oncology are locally or regionally devoted to solving hyperthermia effects in shallow and deep-seated tumours [4]. The problems in these methods are simply connected to the focusing of heat-energy. The energy can be focused by choosing the targeted volume, but due to the non-invasive solutions, the input power is limited by adverse effects, so longer duration is necessary to heat up the target. The longer heating time completely changes the situation; we have to take into account the natural movements of the patient, which heats up the healthy environment, and naturally occurs because of the effective heat-diffusion and heat-conduction in the body. The energy can be focused for longer times to a chosen target volume, but the heat (and the temperature) is not focusable for longer, as it naturally spreads.

The consequences of heat spreading can dramatically change the complete hyperthermia process. The homeostatic regulation of the body tries to re-establish the homeostatic equilibrium. Considering the physiological time-constant (which is a few minutes), the body has negative feedback by increased blood-flow to cool down the heated volume. This effect works against our efforts to heat, and accelerates the spread of the heat. The physiological consequence of the increased blood-flow is more serious than its effect on focusing. The increased blood-flow delivers higher amounts of glucose, supporting the metabolism of cancer cells; also, the intensified transport promotes the

***Corresponding author:** Prof. Szasz Andras, Department of Biotechnics, St. Istvan University. Godollo. Hungary. Tel.: +36-23-555-510; Fax: +36-23-555-515; E-mail: Biotech@gek.szie.hu

Received July 22, 2015; **Accepted** August 31, 2015; **Published** September 07, 2015

Citation: Andocs G, Rehman MU, Zhao QL, Papp E, Kondo T, et al. (2015) Nanoheating without Artificial Nanoparticles Part II. Experimental Support of the Nanoheating Concept of the Modulated Electro-Hyperthermia Method, Using U937 Cell Suspension Model. Biol Med (Aligarh) 7: 247. doi: 10.4172/0974-8369.1000247

dissemination of malignant cells, which invade the blood-stream more easily due to their higher thermal motility. The solution could be when the heating is in the microscopic scale, selecting the malignant cells in the tumour, especially the cell membrane, and its special structural and functional part, the membrane raft. The properly applied RF current is absorbed selectively by the membrane rafts and heated. This special heating mechanism is referred to here as nano-heating. The basic theoretical concept of the nano-heating method was described in detail elsewhere [7].

Modulated electrohyperthermia (mEHT, trade-name oncothermia®) changes the technical paradigm also. It has special selection mechanisms [5] and realises microscopic scale processes [8] on the plasma membrane of the malignant cells. The mEHT method tries to suppress necrotic cell death and induce dominantly programmed (apoptotic) cell death [9]. According to the basic concept of the nano-heating method, it is very different according to the distribution of the temperature during the absorption of energy (Figure 1). It is supposed that the special structural elements of the plasma membrane, membrane rafts, form the centres of membrane-selective heating.

The rafts are special clusters of transmembrane proteins [10,11], with important signalling function [12,13] and interaction with the cytoskeleton [14], bridging physics and biology [15]. Rafts are directly involved in signal transduction [16], and in membrane transport [17], and definitely emphasised in malignant cases [18]. The described concept of cell membrane rafts is well studied nowadays in the relevant literature, and evidence for the existence of lipid rafts in living cells has been recently reported [19].

The electromagnetic properties of rafts are different from those of the other part of the membrane, the lipid bilayer. This difference in electromagnetic properties makes the selective absorption of the applied external RF energy possible, and also enables heating up of the membrane raft protein cluster in the microscopic or even nanoscopic range. Membrane rafts as targets are believed to have a crucial role in the selective microscopic range heating in the mEHT method and was theoretically described elsewhere [7].

The nano-heating method in local hyperthermia has been introduced by locally modulated electro-hyperthermia [20]. It was developed for the treatment of human malignancies [21], and applied in human cancer therapies [22-24]. Intensive basic research was performed to reveal the basic mechanism of action [8,25], as well as the molecular mechanisms of action, which are supposed to be important factors in the mEHT method [26,27]. Despite this huge research effort, however, there are many questions still remaining.

Our objective in this research is to support the theoretical basis of the nano-heating concept using precisely controlled hyperthermia experiments with an *in vitro* cell suspension model system, the U937 (human myelomonocytic lymphoma) cell-line [28]. This cell-line is very sensitive for different apoptosis-inducing factors (heat, radiation, ultrasound) and has been well investigated for various conditions, including thermal effects too [29,30]. The previous studies showed increased intracellular Ca^{2+} concentration to have a crucial role in the apoptosis of U937 cells [31]. The complete mechanism was investigated in detail [32-34], establishing that the temperature-dependent production of free radicals plays an important role in the apoptotic process of U937 [35-37]. Consequently, its further study is the basis of the complex comparative research of thermal processes, which was questioned previously [38]. The investigation method was comparative, measuring the differences between the conventional waterbath hyperthermia treatment (WHT) and mEHT.

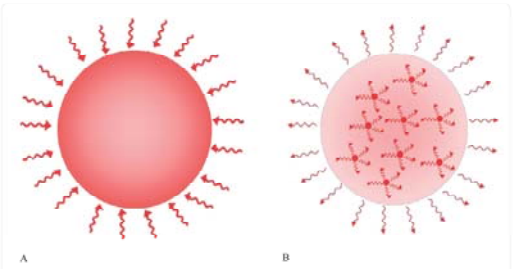

Figure 1: Conventional heating process uses thermal conduction to heat up the complete volume; (A) The heat-flow has a direction from the outer surface to the bulk. In the case of membrane raft selective nano-heating, the heat-source is inside the target (B) so the heat-flow is opposite to that in conventional heating.

Materials and Methods

Cell culture

U937, a human myelomonocytic lymphoma cell line from Human Sciences Research Resource Bank (Japan Human Sciences Foundation, Tokyo, Japan), was used for the experiments. The cells were grown in RPMI 1640 culture medium supplemented with 10% heat-inactivated foetal bovine serum (FBS) at 37°C in humidified air with 5% CO_2. Cells were subcultured every second day, and used for the experiments in their log phase. Cells were treated at a density of 10^6 cells/mL, in a total volume of 8mL.

Treatment processes

Here, 8 mL of U937 cell suspension was used in both of the treatment objects. In the mEHT treatment process, the suspension was pipetted into a coverslip-bottomed slide-flask (Nunc™ Lab-Tek™ II Chambered Coverglass, Thermo Fisher Scientific, Inc., USA) and placed in a special custom-designed platinum electrode applicator, as shown in Figure 2. The pure platinum (99.9%) active RF-electrode was used to minimise electrode by-products. The active electrode was immersed in the cell suspension. The effective surface of this platinum electrode was 10mm x 45mm. The amplitude modulated (AM) 13.56MHz RF source (LabEhy100, Oncotherm, Germany) was connected to the applicator via a precise impedance matching unit. The complete heating-time was 30 minutes for each.

In the case of WHT 8 mL of cell suspension was put in a 15mL centrifuge tube and then placed into a thermoregulated water bath (Thermo Minder SD Mini, Taitek Corp., Japan) continuously measuring the temperature profile throughout the treatment. The complete heating-time was well fit to mEHT, and was 30 min. (Figure 2).

The heating dynamics and the treatment time at maximum temperature were the same in all treatments. After the treatments, cell suspensions were placed in 10 cm diameter plastic Petri dishes (BioBik, Ina-Optika Co. Ltd., Japan) and incubated for 24h. All experiments were performed in triplicate.

Temperature measurement during the heat treatments

The temperature change of the cell suspension during the treatments was assessed by a four-channel fluoroptic temperature measurement system (Luxtron m3300 Biomedical Lab Kit, Lumasense Technologies,

Santa Clara, CA, USA). The temperature measurement probe is an optical fibre that is 0.5 mm in diameter, which is totally insensitive to electromagnetic field. Probes 1 and 2 were used to monitor the temperature changes in the case of WHT, and probes 3 and 4 were used to measure the temperature profile of the mEHT treatment. The probes were precisely positioned on the inner surface of the slide-flask as well as at the lowest point in the centrifuge tube. The measured temperature parameters were recorded real-time (1sampling/sec) using a PC. A representative temperature measurement graph was shown in Figure 3. The isothermal treatments were performed at 39, 40, 41, 42, 43, 44, 45 and 46°C and at 42, 43, 44, and 45°C in mEHT and WHT experiments, respectively.

Morphological detection of apoptosis

To identify the morphological changes of the apoptotic cells after mEHT and WHT, the cells were examined by Giemsa staining. Cells were harvested after 3h and 24h of incubation at 37°C, washed with PBS and collected by centrifugation. Then, the cells were fixed with methanol and acetic acid (3:1) for 24h and spread on the glass slides. After drying, staining was performed with 5% Giemsa solution (pH 6.8) for 20 min, then washed with tap water. The cell samples on the slides were covered by coverslips using Eukitt (O. Kindler GmbH & Co., Germany). Cells were imaged using a conventional bright-field microscope (Olympus BX61 Olympus Corp., Japan) equipped with a standard microscope camera (Olympus DP70, Olympus Corp., Japan).

Live cell imaging

Live cells were imaged using the DIC (differential interference contrast) method with an inverted microscope (Nikon Eclipse, Nikon Corp., Japan) and a conventional DSLR camera (Canon EOS D60).

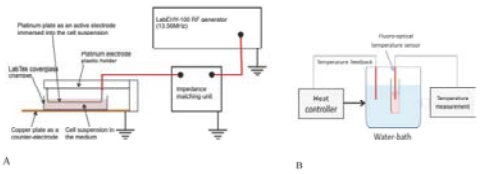

Figure 2: The experimental setups of the hyperthermia treatments mEHT (A) and WHT (B)

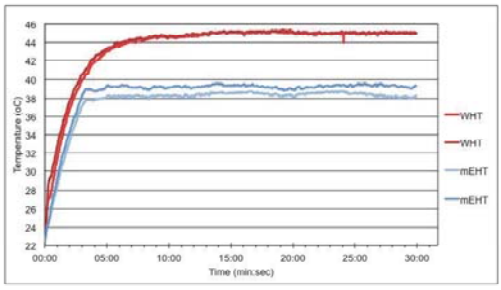

Figure 3: Representative temperature measurement graphs during mEHT and WHT

Detection of apoptosis using Annexin V-FITC/PI staining

To quantitatively investigate the different heat treatment-induced early apoptosis and secondary necrosis, phosphatidylserine (PS) externalisation of apoptosis was determined by analysis of propidium iodide (PI) and fluorescein isothiocyanate (FITC)-labelled Annexin V (Immunotech, Marseille, France) using Flow cytometry (Epics XL, Beckman-Coulter, Miami, FL) [39], according to the manufacturer's instructions. Briefly, followed by the RF and WHT, cells were collected after 3h of incubation at 37°C, washed with cold PBS at 4°C and centrifuged at 1200 rpm for 3 min. The resulting pellet was mixed with the binding buffer of the Annexin V-FITC kit. FITC-labelled Annexin V (5 µl) and PI (5 µl) were added to the 490 µl suspension and mixed gently. After incubation at 4°C for 20 min in the dark, the cells were analysed by flow cytometry.

The dead cell fraction was determined by summarising the apoptotic cell fraction (Annexin V-FITC-positive fraction), the necrotic cell fraction (propidium iodide-positive cell fraction) and the secondary necrotic cell fraction (Annexin V-FITC plus propidium iodide-positive fraction).

In silico models

We assume that membrane lipid rafts have enhanced energy absorption, which create local heating on the surface. The in silico models were created using Computer Simulation Technology software (CST, Darmstadt, Germany). Between two circular parallel plate electrodes with a radius of 1.5 µm a flat membrane with a microdomain (radius of 0.5 µm [40] was placed in the centre. The modelling parameters are shown in Table 1. Thereafter, a seven-cell model was created with seven connection points. The cells had different diameters (10-15 µm) and in the micro-contacts, we assumed the presence of membrane rafts with a uniform 0.1 µm radius and 0.02 µm thickness. Furthermore, the radius and thickness of the two parallel plates were 32 µm and 0.1 µm, respectively, and the distance between them was 56 µm. The material properties of all of these components correspond with the parameters in Table 1.

In both models, the simulating setup was made at 13.56 MHz, using the low-frequency domain solver (Electroquasistatic Solver) of the CST EM Studio. Open boundary conditions were used with a tetrahedral mesh (raft model: 3,247,880 units, 0.005 – 0.13 µm mesh-lines, adaptive division; 7-cell model: 2,538,536 units, 0.0003 – 6.25 µm mesh-lines, adaptive division) with an accuracy of 10^{-6}. The effective potential between the electrodes was 0.1 V (phase-angle: 0°). E-field, Current Density and Electric Loss Density monitors were defined at 13.56 MHz to analyse the electromagnetic field effect.

Results

The live cell images of U937 cells shows the expected densities by differential interference contrast (DIC) (Figure 4.). Quantitative analysis of the cell-death process was performed by flow-cytometry using Annexin V-FITC and PI staining (Figures 5 and 6) and all calculations and further graphs were based on these data.

The careful comparative analysis shows that the U937 cell-line induces significant apoptotic cell-death after the WHT treatment at 44°C, like as shown in earlier studies with treatment durations of 15min [41]. The expected result was reproduced, but the mEHT treatment resulted in a completely different temperature-dependence of cell-death 3h post-treatment. The difference is highly significant (Figure 7) the apoptotic cell death started at a much lower temperature, with a

Parameter category	Values	References
Electrodes (sheets)	PEC (Perfect Electrical Conductor)	
Extracellular (1000 nm)	ε_r=72.5, μ=1, σ=1.2 S/m	[42]
Intracellular (1000 nm)	ε_r=72.5, μ=1, σ=0.3 S/m	[42]
Membrane (5nm)	ε_r=2, μ=1, σ=3*10^{-7} S/m	[42]
Membrane raft (5nm)	ε_r=40, μ=1, σ=3*10^{-6} S/m	[43,44]
Background	ε_r=1, μ=1, σ=0 S/m	

Table 1: The *in silico* parameters used.

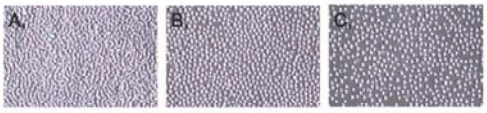

Figure 4: DIC live cell images of U937 cells in the treating chamber at various cell densities (A, 1x10^6 cells/mL, B, 0.25x10^6 cells/mL, and C, 0.125x10^6 cells/mL).

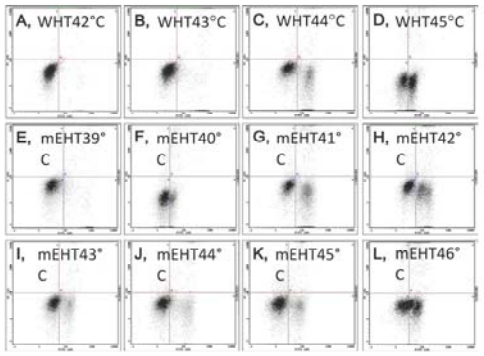

Figure 5: Representative collection of the flow-cytometer plots of the Annexin V–FITC and PI measurements of the treated cell samples. A: WTH42°C, B: WTH43°C, C: WTH44°C, D: WTH45°C; E: mEHT39°C, F: mEHT40°C, G: mEHT41°C, H: mEHT42°C; I: mEHT43°C, J: mEHT44°C, K: mEHT45°C, L: mEHT46°C.

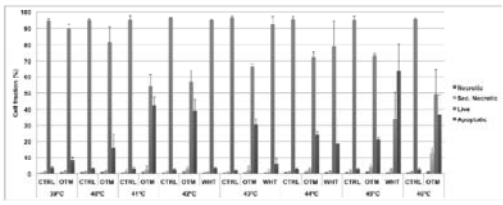

Figure 6: Quantitative data of the flow-cytometer analysis of the Annexin V–FITC and PI measurements of the treated cell samples. Averaged data of three independent experimental series.

difference of about 3°C. The definite difference between the two kinds of heating processes is more obvious in the higher temperature treatments by MEHT. The cell-death increased by temperature until 41°C, but after this it decreased with increasing temperature, and started to rise again only at 45°C (Figure 8). The similarity of WHT at 45°C and mEHT at 41°C was clearly shown by Giemsa staining of treated cells, 3h post-treatment (Figure 8), showing the same stages as the live cell DIC microscopy. The morphology in Giemsa-stained microscopy images (Figure 9), 3h post-treatment showed typical morphological signs of apoptotic cell death, dominantly in WHT at 45°C (Figure 8D) and mEHT at 41°C (Figure 8G). The in silico modelling clearly showed the special high-field (Figure 10) and high energy-absorption (Figure 11) places on the cell-membrane at the membrane rafts.

The absolute component of the current density was visualised in a 2D plot (Figure 12). The results showed peculiar current density peaks at the raft–membrane interface due to the high permittivity and conductivity of the lipid raft domain. Strong electric loss can be discovered in the local environment of the membrane raft based

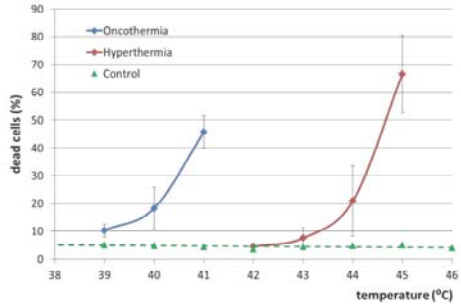

Figure 7: Comparison of cell-death-amount (%) of the two different heating methods 3 hours after the process, measured by Annexin PI. Every point is measured in three independent experiments, and the arithmetic average is shown. The error-bars are the standard deviations of the data-sets.

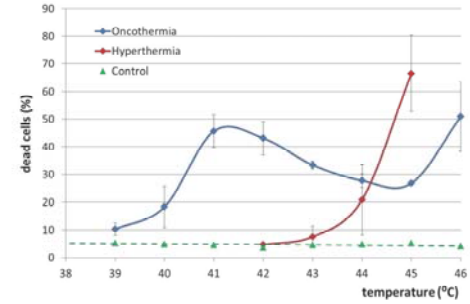

Figure 8: Extended comparison of cell-death-amount (%) of the two different heating methods 3 hours after the process, measured by Annexin PI. The measured values for mEHT in higher temperature points are shown. Every point was measured in three independent experiments, and the arithmetic average is shown. The error-bars are the standard deviations of the data-sets.

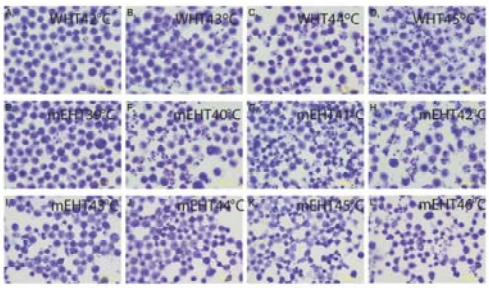

Figure 9: Representative morphological images of the fixed and Giemsa-stained treated cells, 3h post-treatment. A: WHT42°C, B: WHT43°C, C: WHT44°C, D: WHT45°C; E: mEHT39°C, F: mEHT40°C, G: mEHT41°C, H: mEHT42°C, I: mEHT43°C, J: mEHT44°C, K: mEHT45°C, L: mEHT46°C

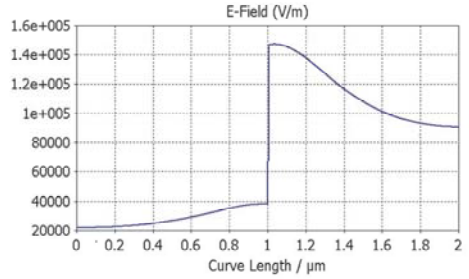

Figure 10: Distribution of electric field perpendicular to the membrane in membrane raft (V/m). The raft position is in 1-1.005 µm interval. The extra- and intracellular electrolytes are shown on the left and right, respectively.

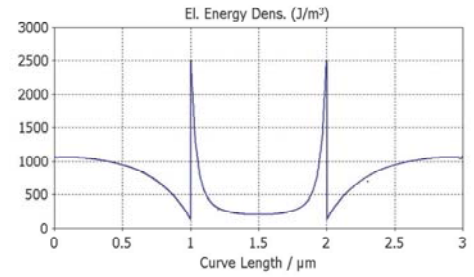

Figure 11: Distribution of absorbed energy in the plane of the membrane (J/m³). The raft is placed in the 1-2 µm position.

on computer simulations (Figure 13). One order of magnitude loss differences are generated at the cell membranes by the lateral inhomogeneity. This concentrated energy loss is that part of the energy which is able to transform into heat loss and can cause local hot spots.

The simulation results in the seven-cell model (where the intercellular contacts are membrane raft units), which presents high

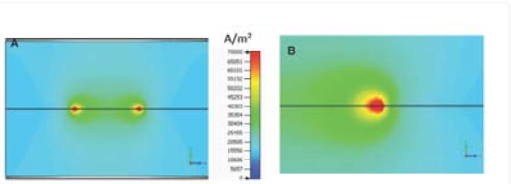

Figure 12: The current density in x=0 plane (A) magnified by 3 times (B). The upper half is extracellular, while the lower half is intracellular.

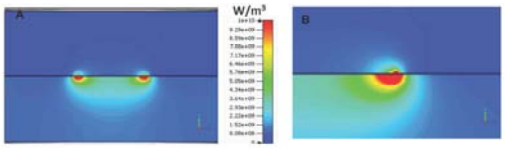

Figure 13: The electric loss in x=0 plane (A) magnified by 3 times (B). The upper half is extracellular, while the lower half is intracellular.

local electric loss peaks at the intercellular connections, especially in the vertical cell contacts (Figure 14). This model confirms the increasing cell death rate, and the decreasing rate after a while too, when the cell group number reduces due to cell damage.

Discussion

The cell-destruction by mEHT starts at a significantly lower temperature than by WHT (Figure 6). This remarkable shift in temperature in favour of mEHT vs. conventional infrared hyperthermia was previously shown in an animal tumour model study [45].

The supposed reason is the different microscopic effects, which have the same macroscopic average of energy at the end, but the distribution during the processes is completely different [46]. The explanation is generally based on the electromagnetic differences of the various electrolytes in the tissue, and the RF energy targets the membrane, especially the membrane rafts of the malignant cells, selectively. The recent results could explain the mechanism of the selective RF energy absorption in more detail, taking into account the inhomogeneity of the membranes and its high electrical conductive membrane raft parts which could be highly loaded with absorbed energy, supporting the nano-heating effect which was described earlier [26,7].

In our case, the two different heating processes act very differently in the non-homogeneous media. The waterbath heats with a macroscopic gradient from the surface of the flask to its middle, while the mEHT starts in depth, heating first the selected membrane rafts and meaning that the heat-flow direction is opposite in mEHT than in the WHT (Figure 1). The cellular heating in the case of mEHT originated from the membrane-rafts, the vicinity of which absorbs high energy (Figure 10), and its current density (Figure 11) and energy absorption (dielectric loss, Figure 12) are significantly higher than those in the neighbouring membrane.

Consequently, the shift in overall temperature value shows an important factor of the hyperthermia treatments in general: the same average temperature is not sufficient to characterise the complete process, but the distribution of SAR certainly modifies this. As a result, the hyperthermia in oncology must be identified not only by the

temperature and its duration, but also by the method in which it was applied.

The other important observation from the lower temperature effects of MEHT is the fact that the shapes of the curves are similar (Figure 6); expecting the same overall thermal character. The measured effects are significantly different: their error-bands have no overlapping (Figure 15).

The Arrhenius plot shows the thermal character of both of the measurements; both of the actual reactions are clearly dependent on the reciprocal value of the absolute temperature (Figure 16). Consequently, both processes are certainly thermal; however, their activation energies (E_a) are different: the value is approximately 20% lower in the case of mEHT (Table 2).

The suppression of cellular death by increasing temperatures between 41°C and 45°C in the mEHT treatment could be explained by a special clustering effect of the cells [1]. The suspension cell culture allows the free movement of the cells. When the cells are approaching each other in the outer electric field, attractive forces are induced between them, creating temporary cell to cell contacts with each other [47].

Despite the same charge being on their outer membrane surface, the cell-cell contacts are created, orienting the cells by the dielectrophoretic forces [48]. The effective distance of such cell-cell contacts (in case of erythrocytes) was found to be 5-10 μm [49]. The outer electric field helps to orient the membrane rafts [50], which easily move in the membrane direction, and make contacts by their ligands between the cells [51].

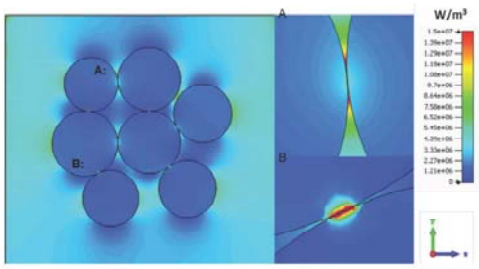

Figure 14: The electric loss of 7-cell model in x=0 plane. Right: figures correspond to the marked cell connections magnified by 64 times (A and B). The intercellular contact points are membrane raft units which present high local electric loss peaks, especially in the vertical cell contacts.

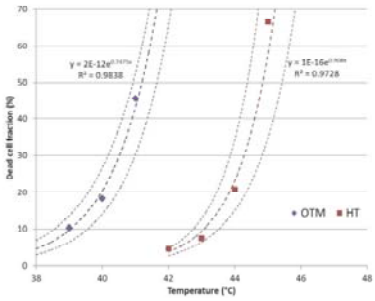

Figure 15: Error-bands of the measured data. The dashed lines show the fits of the minimal and maximal data of every measured set of points.

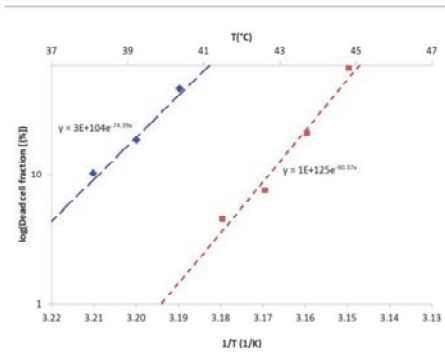

Figure 16: Arrhenius plot of the data

Treatment	Frequency factor	E_a/R [K/mol]
MEHT	$3 \cdot 10^{104}$	74.39
WHT	$1 \cdot 10^{125}$	90.37

Table 2: Measured Arrhenius parameters (R≈8.3 J/mol/K, is the universal gas-constant).

The intercellular contact points make high RF-current density (Figure 17), which was proved by the computer simulation (Figure 13). This high RF current density and the higher absorbed RF energy in these contacting membrane regions start to destroy the membrane and initiate apoptotic cell death. The inhomogeneous temperature distribution makes the shift of the cell-death-rate between the mEHT and WHT (Figure 17).

The mEHT treatment overheats the intercellular contacting points and induces the membrane destruction when the temperature is sufficient for that membrane modification. However these contacts reach a high temperature earlier that the average temperature shows. These contact points are hotter by at least 3°C. However, the temperature increase starts to disconnect the contacting cells, producing additional unconnected cells in the suspension. The normal thermal processes start to act, and the special hotspots decrease, suppressing the exceptional membrane damage. In accordance with our model of nano-heating, the large membrane distortion is less than the starting one.

Cells have multiple contacting points which have high RF current density; consequently their SAR is extremely high. As the temperature increases in the mEHT treatment, the number of intercellular contact points decreases and the influence of the nanoheating effects on these contact points and the cell destruction rates also decrease, meaning that the situation is more similar to the normal WHT treatment conditions. In high enough temperatures (around 44°C) the clusters are completely dissolved, and the cells will be heated without microcontact spots (Figure 18). This theory is clearly supported by the additional experiments which were carried out at 41°C using lower cell densities (0.5 x10^6 cells/mL, 0.25 x10^6 cells/mL and 0.125 x10^6 cells/mL) than the original density of 1 x10^6 cells/mL. The dead cell ratio was significantly lower

at this temperature range when mEHT treatment was carried out at a lower cell density (data not shown). The outside electric field curves the membrane at the raft-bond, and the curvature stabilises the membrane raft domains in the lipid bilayers [52,53], which fixes the contact points until the higher temperature does not break it. The thermal processes in hyperthermia are generally described by Arrhenius plots [54]. The proposed reference temperature in the hyperthermia dose is 43°C [55], which is also determined by the Arrhenius thermal actions [2], and the dose function for clinical use is also based on this thermal effect [56].

As shown here, the complete thermal membrane process fits the Arrhenius plot well. This fact determines the category of the effect on the membrane: it has thermal origin. It was previously shown [57,58] that the established adherent connections also have Arrhenius dynamics, where the E_a activation-energy is lowered by an energy factor that is characteristic of the active connection. The present down-shifting of the lethal temperature in the hyperthermia effect clearly proves the growth of cell-killing efficacy by the nano-range heating.

The mEHT process can be fitted by the two Arrhenius exponentials (the mEHT initial with large clustering case, and late mEHT with mono-cellular structure), and the cluster effect can be fitted by its normal distribution (Figure 19). The clustering of cells is spread by the higher temperature (here fit by a Gaussian distribution), and the individual cells start to behave as the WHT forces them to.

The complete heating process could be fitted into the thermal-scheme by Arrhenius functions. The heating periods in both treatment modalities are characterised by the Arrhenius parameters, but the decomposition of the clusters behaves in the opposite way. This opposite trend is also definitely thermal. At the end, the mEHT became classical thermal, fitting the earlier measured points of the WHT process very well (Figure 20).

These experiments were performed on U937, a human myelomonocytic lymphoma cell line. These cells are well autonomic, and so the cellular connections (cadherins, junctions, etc.) do not characterize this system. This is the supposed case for all the malignant cells lines, where the functional cell-cell connections are negligible.

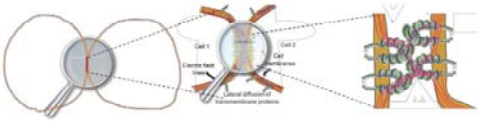

Figure 17: The RF-current density could be extremely high at the intercellular contacting points. The high density current causes high energy deposition in the spots and heats this to a higher temperature than its environment

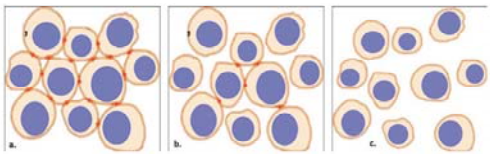

Figure 18: Schematic representation of the nanoheating effect of the intercellular contacting points at various cell densities (a) dense arrangement, frequent cell-contact, (b) medium cell density few cell-contacts (c) low cell-density, rare cell-contacts. These considerations are well supported by the DIC live image observations shown in **Figure 4.**

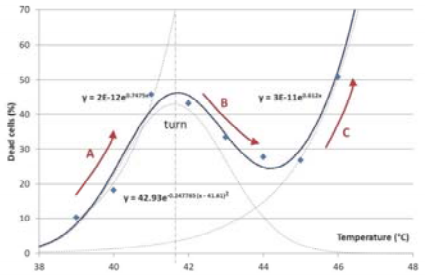

Figure 19: Fits for the mEHT treatment in temperature (°C) plot. The initial curve describes the state when a large number of intercellular contacting points exist in the suspension cell culture and their high membrane temperature induced by the nanoheating effect, showing the xponential development of cell-killing (A slope), while at a turning point (at about 41.5°C), the rapid decrease in the number of intercellular contacting points show a decrease of the cell-killing rate (B slope), and at high temperature the individual cells are destroyed by conventional thermal equilibrium (C slope).

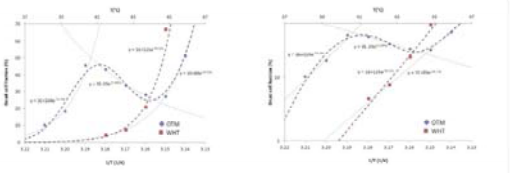

A B

Figure 20: The mEHT treatment in temperature (°C) plot in linear scale (A) and in logarithmic scale (B)

Conclusion

In this paper, using a very simple experimental series, we showed that mEHT-induced cell-killing effects are thermal in nature. This satisfies the definitive thermal character by Arrhenius plot. It is important to see that the mEHT nanoheating mechanism made hot-spots in the intercellular contact points in the U937 suspension cell-culture, which allowed cell-destruction at temperatures that were about 3°C lower than with WHT. As the temperature increased, the thermal properties of intercellular contacting points suppressed this "early effect" and the cell destruction rate decreased until 44°C. Above this temperature range, the direct cell killing effect of the high temperature started to dominate and the cell destruction rate of mEHT and WHT changed together. The detailed molecular mechanism of the nanoheating effect is under intensive investigation, the results of which will be presented in our next research paper.

References

1. Hyperthermia definition
2. Sapareto SA, Dewey WC (1984) Thermal dose determination in cancer therapy. Int J Radiat Oncol Biol Phys 10: 787-800.
3. Szasz A, Iluri N, Szasz O (2013) Local hyperthermia in oncology – To choose or not to choose? book ed. Huilgol N. Hyperthermia, Intech, Hungary.
4. Szasz A, Szasz O, Szasz N (2006) Physical background and technical

realization of hyperthermia, By Baronzio GF, Hager ED. Hyperthermia in cancer treatment: A primer, Springer, Landes Biosceince.

5. Szasz A (2013) Challenges and solutions in oncological hyperthermia, Thermal Med 29:1-23.
6. Mori S, Aravalli R, Choi J, Cressman E, Bishof J (2011) Importance of Protein Denaturation to Thermochemical Ablation of Liver Tumors, ASME 2011 Summer Bioengineering Conference, 119-120.
7. Vincze Gy, Szigeti Gy, Andocs G, Szasz A (2015) Nanoheating without artificial nanoparticles, Part I Theoretical consideration. Co-submitted with the present paper.
8. Szasz O, Szasz A (2014) Oncothermia – Nano-heating paradigm, J Cancer Sci Ther 6:117-121.
9. Meggyeshazi N, Andocs G, Balogh L, et al (2014) DNA fragmentation and caspase-independent programmed cell death by modulated electrohyperthermia, Strahlenther Onkol 190:815-822.
10. Karnovsky MJ, Kleinfeld AM, Hoover RI, Klausner RD (1982) The concept of lipid domains in membranes. J Cell Biol, 94:1-6.
11. Simons K, Ikonen E (1997) Functional rafts in cell membranes. Nature 387:569-572.
12. Brown D (2002) Structure and function of membrane rafts. Int J Med Microbiol 291: 433-437.
13. Head BP, Patel HH, Insel PA (2013) Interaction of membrane/lipid rafts with the cytoskeleton: Impact on signalling, and function; Membrane/lipid rafts, mediators of cytoskeletal arrangement and cell signalling, Biochim Biophys Acta 1838:532-545.
14. Gurunadh R. Chichili, Rodgers W (2009) Cytoskeleton-membrane interactions in membrane raft structure. Cell Mol Life Sci 66:2319-2328.
15. Foster KR, Schepps JL (1981) Dielectric properties of tumour and normal tissues at radio through microwave frequencies. J. Microwave Power 16:107-119.
16. Brown DA, London E (1998) Functions of lipid rafts in biological membranes. Annu Rev Cell Dev Biol 14: 111-136.
17. Ikonen E (2001) Roles of lipid rafts in membrane transport. Curr Opin Cell Biol 13: 470–477.
18. Wirtz D, Staunton Jr PC-OC (2013) The Physical Sciences-Oncology Centres Network. A physical sciences network characterization of non-tumorigenic and metastatic cells. Sci Rep 3:1449.
19. Gaus K, Gratton E, Kable EP, Jones AS, Gelissen I, et al. (2003) Visualizing lipid structure and raft domains in living cells with two-photon microscopy. Proc Natl Acad Sci U S A 100: 15554-15559.
20. Szasz A, Szasz N, Szasz O (2010), Oncothermia Principles and Practices, Springer, Dordrecht, Heidelberg.
21. Andocs G, Szasz O, Szasz A (2009) Oncothermia treatment of cancer: from the laboratory to clinic. Electromagn Biol Med 28: 148-165.
22. Hager ED, Dziambor H, Höhmann D, Gallenbeck D, Stephan M, et al. (1999) Deep hyperthermia with radiofrequencies in patients with liver metastases from colorectal cancer. Anticancer Res 19: 3403-3408.
23. Wismeth C, Dudel C, Pascher C, Ramm P, Pietsch T, et al. (2010) Transcranial electro-hyperthermia combined with alkylating chemotherapy in patients with relapsed high-grade gliomas: phase I clinical results. J Neurooncol 98: 395-405.
24. Gadaleta-Caldarola G, Infusino S, Galise I, Ranieri G, Vinciarelli G, et al. (2014) Sorafenib and locoregional deep electro-hyperthermia in advanced hepatocellular carcinoma: A phase II study. Oncol Lett 8: 1783-1787.
25. Andocs G, Meggyeshazi N, Balogh L, et.al (2015) Up-regulation of heat shock proteins and the promotion of damage-associated molecular pattern signals in a colorectal cancer model by modulated electrohyperthermia. Cell Stress Chaper 20:37-46.
26. Szasz A (2013) Electromagnetic effects in nanoscale range, chapter 4 in book ed. Shimizu T, Kondo T. Cellular response to physical stress and therapeutic application, Nova Science Publishers, Inc.
27. Hegyi G, Szigeti GyP, Szasz A (2013) Hyperthermia versus Oncothermia: Cellular effects in cancer therapy, Evidence based Compliment Alternat Med 2013: 1-12.
28. Sundström C, Nilsson K (2006) Establishment and characterisation of a human histiocytic lymphoma cell line (U-937). Int J Cancer 17: 565-577.
29. Arai Y, Kondo T, Tanabe K, Zhao QL, Li FJ, et al. (2002) Enhancement of hyperthermia-induced apoptosis by local anesthetics on human histiocytic lymphoma U937 cells, J Biol Chem 277: 18986-18993.
30. Cui ZG, Kondo T, Matsumoto H (2006) Enhancement of apoptosis by nitric oxide released from alpha-phenyl-tert-butyl nitrone under hyperthermic conditions. J Cell Physiol 206:468-476.
31. Kameda K, Kondo T, Tanabe K, Zhao QL, Seto H (2001) The role of intracellular Ca(2+) in apoptosis induced by hyperthermia and its enhancement by verapamil in U937 cells, Int J Radiat Oncol Biol Phys 49:1369-1379.
32. Li M, Kondo T, Zhao QL, Li FJ, Tanabe K, et al. (2000) Apoptosis induced by cadmium in human lymphoma U937 cells through Ca2þ- calpain and caspase-mitochondria-dependent pathways. J Biol Chem 275:39702-39709.
33. Zhao QL, Fujiwara Y, Kondo T (2006) Mechanism of cell death induction by nitroxide and hyperthermia. Free Radic Biol Med 40: 1131-1143.
34. Li FJ, Kondo T, Zhao QL, Hayashi Y, et al (2003) A lipophilic free radical initiator, 2,20-azobis (2,4-dimethylvaleronitrile) (AMVN) enhances caspase-dependent apoptosis induced by hyperthermia. Int J Hypertherm 19:165-177.
35. Li FJ, Kondo T, Zhao QL, Tanabe K, Ogawa R, et al. (2001) Enhancement of hyperthermia induced apoptosis by a free radical initiator, 2,2'-azobis(2-amidinopropane) dihydrochloride, in human histiocytic lymphoma U937 cells. Free Radic Res 35:281-299.
36. Wada S, Cui ZG, Kondo T, Zhao QL, Oqawa R, et al (2005) A hydrogen peroxide generating agent, 6-formylpterin, enhances heat-induced apoptosis. Int J Hyperthermia 21:231-246.
37. Katschinski DM, Boos K, Schindler SG, Fandrey J (2000) Pivotal role of reactive oxygen species as intracellular mediators of hyperthermia-induced apoptosis. J Biol Chem 275: 21094-21098.
38. Feril LB Jr, Kondo T, Zhao QL, Ogawa R (2002) Enhancement of hyperthermia-induced apoptosis by non-thermal effects of ultrasound. Cancer Lett 178: 63-70.
39. Cui ZG, Kondo T, Feril LBJ, Waki K, Inanami O, Kuwabara M (2004) Effects of antioxidants on X-ray- or hyperthermia-induced apoptosis in human lymphoma U937 cells. Apoptosis 9:757-763.
40. Dharia S (2011) Spatially and temporally resolving radio-frequency changes in effective cell membrane capacitance, Dissertation.
41. Furusawal Y, Tabuchi Y, Wada S, Takasaki I, Ohtsuka K, et al. (2011) Identification of biological functions and gene networks regulated by heat stress in U937 human lymphoma cells, International. J Mol Med 28:143-151.
42. Kotnik T, Miklavcic D (2000) Theoretical Evaluation of the Distributed Power Dissipation in Biological Cells Exposed to Electric Fields, Bioelectromagnetics, 394:385-394.
43. Pitera JW, Falta M, van Gunsteren WF (2001) Dielectric properties of proteins from simulation: the effects of solvent, ligands, pH, and temperature. Biophys J 80: 2546-55.
44. Banerjee S, Vandenbranden M, Ruysschaert J (1981) Interaction of tobacco mosaic virus protein with lipid membrane systems. FEBS Lett 133: 221-224.
45. Andocs G, Renner H, Balogh L, Fonyad L, Jakab C, et al. (2009) Strong synergy of heat and modulated electromagnetic field in tumor cell killing. Strahlenther Onkol 185: 120-126.
46. Szasz A, Szasz N, Szasz O (2010) Oncothermia Principles and Practices, Springer, Dordrecht, Heidelberg; Heating the extracellular electrolyte, Chapter 4.1.11. 205-208.
47. Liu Y, Liu WK, Belytschko T, Patankar N, To AC, Kopacz A, Chung JH (2007) Immersed electrokinetic finite element method, Int. J. Numer. Methods Eng 71:379-405.
48. Pollock JK, Pohl DG (1988) Emission radiation by Active Cells. In: Fröchlich H. Biological Coherence and Response to External Stimuli. Springer Verlag, UK.
49. Rowlands S, Sewchand LS, et al (1998) A Fröchlich interaction of human erythrocytes. Phys Lett 82:436-438.
50. Szasz A, Szasz N, Szasz O (2010) Oncothermia Principles and Practices,

Springer, Dordrecht, Heidelberg;, Components of cell-destruction, Appendix 30: 470-471.

51. Murai T (2012) The role of lipid rafts in cancer cell adhesion and migration, Intl J Cell Biol 2012: 1-6

52. Meinhardt S, Vink RLC, Schmid F (2013) Monolayer curvature stabilises nanoscale raft domains in mixed lipid bilayers. Proc Natl Acad Sci 110:4476-4481.

53. Meinhardt S (2013) Curvature-induced nanoscale rafts in lipid membranes, Johannes Gutenberg-University Mainz; PhD dissertation.

54. Pearce JA (2013) Thermal dose models: Irreversible alterations in tissues, In: Physics of Thermal Therapy, Ed. Moros EG. CRC Press 23-40.

55. Perez CA and Sapareto SA (1984) Thermal dose expression in clinical hyperthermia and correlation with tumor response/control. Cancer Res 44:4818s-4825s.

56. Thrall DE, Rosner GL, Azuma C, Larue SM, Case BC, et al. (2000) Using units of CEM43oC T90 local hyperthermia thermal dose can be delivered as prescribed. Int J Hyperthermia 16:415-428.

57. Szasz A (2007) Hyperthermia, a modality in the wings. J Cancer Res Therapeut 3:56-66.

58. Szasz A, Vincze G (2006) Dose concept of oncological hyperthermia: heat-equation considering the cell destruction. J Cancer Res Ther 2: 171-181.

Citation: Andocs G, Rehman MU, Zhao QL, Papp E, Kondo T, et al. (2015) Nanoheating without Artificial Nanoparticles Part II. Experimental Support of the Nanoheating Concept of the Modulated Electro-Hyperthermia Method, Using U937 Cell Suspension Model. Biol Med (Aligarh) 7: 247. doi: 10.4172/0974-8369.1000247